arXiv:1604.04254v2 [astro-ph.HE] 23 May 2016

DYNAMICAL FORMATION OF THE GW150914 BINARY BLACK HOLE

Carl L. Rodriguez[1], Carl-Johan Haster[2], Sourav Chatterjee[1], Vicky Kalogera[1], and Frederic A. Rasio[1]

[1]Center for Interdisciplinary Exploration and Research in Astrophysics (CIERA) and Dept. of Physics and Astronomy, Northwestern University 2145 Sheridan Rd, Evanston, IL 60208, USA

[2]School of Physics and Astronomy, University of Birmingham, Birmingham, B15 2TT, United Kingdom

ABSTRACT

We explore the possibility that GW150914, the binary black hole merger recently detected by Advanced LIGO, was formed by gravitational interactions in the core of a dense star cluster. Using models of globular clusters with detailed N-body dynamics and stellar evolution, we show that a typical cluster with a mass of $3 \times 10^5 M_\odot$ to $6 \times 10^5 M_\odot$ is optimal for forming GW150914-like binary black holes that will merge in the local universe. We identify the most likely dynamical processes for forming GW150914 in such a cluster, and we show that the detection of GW150914 is consistent with the masses and merger rates expected for binary black holes from globular clusters. Our results show that dynamical processes provide a significant and well-understood pathway for forming binary black hole mergers in the local universe. Understanding the contribution of dynamics to the binary black hole merger problem is a critical step in unlocking the full potential of gravitational-wave astronomy.

Keywords: globular clusters: general — stars: black holes — gravitational waves

1. INTRODUCTION

The first detection of gravitational waves from merging black holes (Abbott et al. 2016a) has begun a new era of astronomy. GW150914 carried with it profound implications for many astrophysical models of black hole (BH) formation throughout cosmic time. The surprisingly large masses of the individual BH components ($36 M_\odot$ and $29 M_\odot$) strongly suggest that the binary BH (BBH) progenitor of GW150914 was formed in a low-metallicity environment (Abbott et al. 2016, and references therein). Theoretical studies have shown that dynamical interactions in the dense cores of low-metallicity globular clusters (GCs) are particularly efficient at forming BBH systems similar to GW150914 (Rodriguez et al. 2016; Chatterjee et al. 2016).

Shortly after the formation of a GC, the most massive stars collapse, leaving behind a population of BHs. Being more massive than the typical star, these BHs rapidly sink into the center of the cluster, where the tremendous spatial density of BHs ($\sim 10^6$ pc^{-3}) can produce many encounters between BHs and BH binaries. These encounters can create new binaries in one of two ways: either three single BHs pass sufficiently close to one another for two BHs to become bound (with the third BH receiving a velocity boost to conserve energy), or an exchange interaction occurs in which a BH inserts itself into a preexisting binary, ejecting one of its components. The newly-forged binaries remain in the GC core, where they are continuously modified, disrupted,

and recreated by encounters with other binary and single BHs. This dynamical mosh pit continues, forming more and more strongly bound binaries (Heggie 1975) until a BBH receives a sufficient velocity kick to eject it completely from the cluster. In effect, the extreme density of BHs in a GC core creates a veritable gravitational-wave factory, continuously forming and ejecting BBHs into the field to await their fate as Advanced LIGO sources.

In this letter, we explore the dynamical formation channel for BBHs in the context of GW150914. In Section 2, we explore what type of present-day GC could have formed the GW150914 BBH. In Section 3, we show what type of interactions in a GC are responsible for the dynamical formation of GW150914-like binaries. Finally, in Section 4, we show that the GW150914 detection is consistent with the masses and redshifts of BBHs from GCs that we expect Advanced LIGO to detect.

To answer these questions, we use 48 detailed star-by-star GC models, developed in Rodriguez et al. (2016), which incorporate all the relevant dynamical physics and advanced algorithms for stellar evolution, equivalent to the most recent studies of BBH mergers from galactic fields (Dominik et al. 2013). These models span large ranges in initial masses ($N = 2 \times 10^5$, 5×10^5, 1×10^6, and 2×10^6 initial particles, corresponding to present-day masses of $\sim 5 \times 10^4 M_\odot$, $1 \times 10^5 M_\odot$, $3 \times 10^5 M_\odot$, and $6 \times 10^5 M_\odot$, respectively), stellar metallicities ($0.25 Z_\odot$, $0.05 Z_\odot$, and $0.01 Z_\odot$), and initial virial radii (1 pc and 2 pc). See Appendix A for more details.

2. FORMING HEAVY BBHS IN GCS

We extract from our 48 models all the binaries that appear similar to GW150914. We start by looking at any BBH whose source-frame component and chirp masses fall within the 90% credible regions for GW150914 ($m_1 = 35.7^{+5.4}_{-3.8}M_\odot$, $m_2 = 29.1^{+3.8}_{-4.4}M_\odot$, and $\mathcal{M}_c = 27.9^{+2.1}_{-1.7}M_\odot$, from The LIGO Scientific Collaboration & The Virgo Collaboration 2016b). This corresponds to a total of 262 BBHs from 40 of the 48 GC models, 259 of which merge outside the cluster. We assume all GCs formed ~ 12 Gyr ago (at $z \simeq 3.5$, consistent with GCs in the Milky Way, although other galaxies, such as the Large and Small Magellanic Clouds, have significantly younger GC populations). Of the 8 GC models that do not contribute BBHs with masses like GW150914, 4 have disrupted before 12 Gyr and are exlcuded from our analysis, and the remaining 4 have low initial N and lower number of initial BHs. The remaining 40 GC models contribute roughly equal numbers of GW150914-like BBHs (when normalized to the number of initial stars in each model). Our models show a strong dependence on metallicity, with the $Z = 0.05Z_\odot$ and $0.01Z_\odot$ models contributing nearly 3 and 5 times as many BBHs as the $Z = 0.25Z_\odot$ models, respectively.

We then define a true GW150914 progenitor to be the subset of these 262 binaries that merge between 7 and 13 Gyr after GC formation, corresponding to mergers that occur in the local universe ($z < 0.5$). We find 14 such systems across our 48 models, all of which were ejected from the cluster prior to merger. Of these 14, we find that 10 originate from 5 GC models with similar initial conditions, corresponding to GCs with lower metallicities ($0.05Z_\odot$ and $0.01Z_\odot$, typical for the low-metallicity clusters in most galaxies), large masses ($N = 1 \times 10^6$ and 2×10^6 initial particles, corresponding to final masses of $3 \times 10^5 M_\odot$ to $6 \times 10^5 M_\odot$ today), and typical virial radii ($R_v = 2$ pc). That these binaries (and the majority of all 262 GW150914-like BBHs) form from low metallicity and massive clusters is unsurprising: lower metallicities yield less effective stellar winds (Vink 2011), reducing the amount of mass that is lost before a massive star collapses, and producing "heavy" BHs like the observed components of GW150914 (Belczynski et al. 2010; Mapelli et al. 2013; Spera et al. 2015). Furthermore, massive clusters produce a larger number of BHs, which enhances the dynamical production of BBHs.

The preference for clusters with larger virial radius (2 pc versus the more compact 1 pc clusters) arises from the need for long inspiral times. Binaries with total masses of $\sim 60M_\odot$ are more massive than the average stellar or BH mass in the cluster, and are typically ejected within the first few Gyrs of a cluster's evolution. However, since
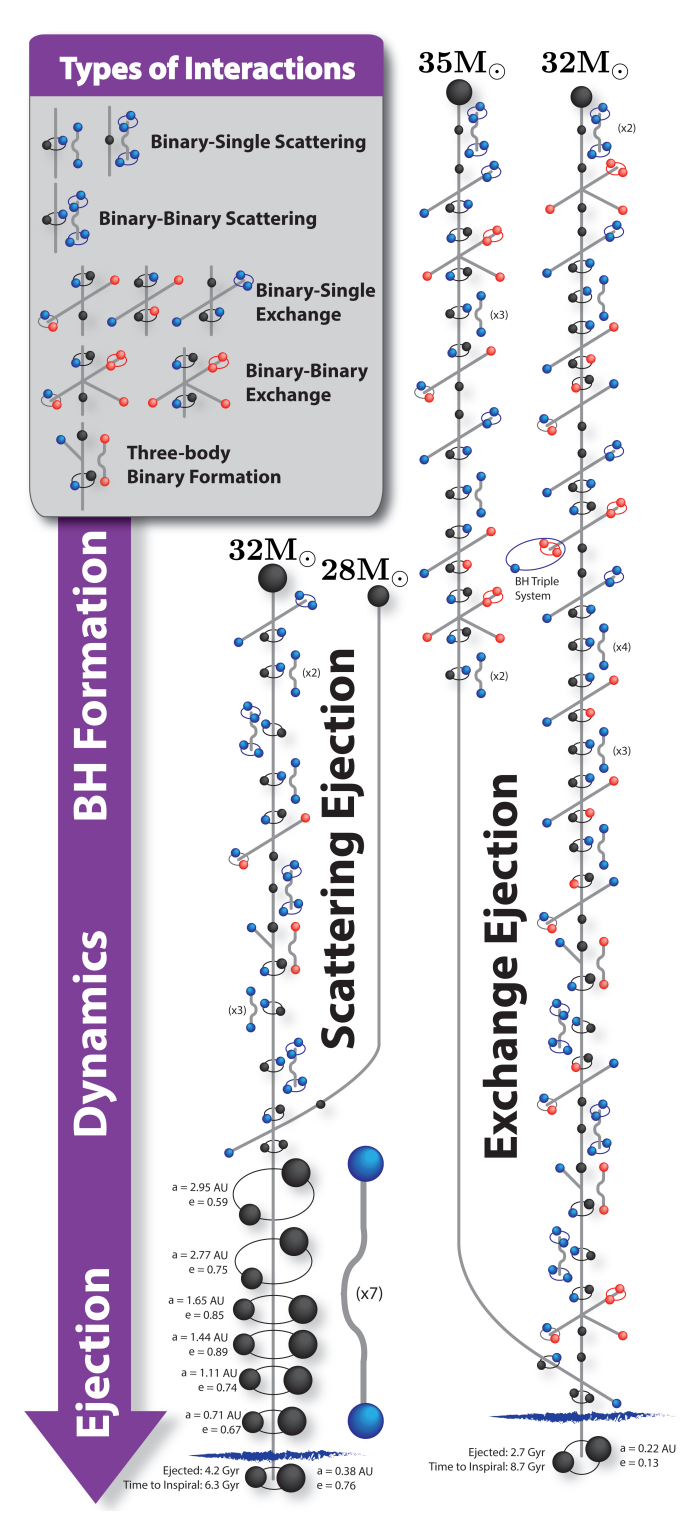

Figure 1. Interaction diagram showing the formation history for two GW150914 progenitors in a single GC model. From top to bottom, the history of each individual BH that will eventually comprise a GW150914-like binary is illustrated, including all binary interactions. The legend shows the various types of gravitational encounters included in our GC models (with the exception of two-body relaxation). In each interaction, the black sphere represents the GW150914 progenitor BH, while the blue and red spheres represent other BHs (and stars) in the cluster core.

GW150914 merged ~ 1.3 Gyr ago ($\gtrsim 10$ Gyr after the formation of the old GCs considered here), it must have been ejected from a cluster environment with a sufficiently wide separation to ensure a delay time of ~ 10 Gyr before merger. It is a well-known result (Portegies Zwart & McMillan 2000; Moody & Sigurdsson 2009) that, despite the chaotic nature of dynamical formation, it is the global cluster properties that primarily determine the semi-major axis of binaries at ejection. In Rodriguez et al. (2016), we showed that this relationship can be expressed as

$$\frac{R_v}{M_{GC}} \sim \frac{a}{\mu_{\rm bin}} \qquad (1)$$

where M_{GC} and R_v are the mass and virial radius of the cluster, and a and $\mu_{\rm bin}$ are the semi-major axis and reduced mass of the binary. Equation (1) shows that, for a given binary mass, more massive clusters must have large virial radii to produce binaries with large semi-major axes[1]. This result holds true in our models: the massive GCs with $R_v = 1$ pc produce $\sim 60 M_\odot$ BBHs at a rate similar to GCs with $R_v = 2$ pc; however, the majority of binaries from those compact clusters are ejected within the first Gyr of the cluster evolution and merge $\lesssim 1$ Gyr later. For the binaries to merge in the local universe, they were most likely ejected from a massive cluster with a virial radius ~ 2 pc. We conclude that, were it formed dynamically, the progenitor of GW150914 most likely originated in a low-metallicity GC with a present-day mass between $3 \times 10^5 M_\odot$ and $6 \times 10^5 M_\odot$ and an initial virial radius of 2 pc, typical of young clusters in the local universe (e.g., Scheepmaker et al. 2007).

3. DYNAMICAL FORMATION OF GW150914

In addition to the statistics of the ejected BBHs, our GC models allow us to describe the specific dynamical interactions that created a potential GW150914 BBH. None of our 14 GW150914 progenitors are formed from primordial stellar binaries that become BBHs, and only 12 of all 262 binaries with GW150914-like masses are formed directly from a primordial binary. Instead, all but one of the 14 progenitors were created during a strong gravitational exchange encounter involving either one binary and one single BH (in 11 cases) or two BBHs (in 2 cases). Only one binary was created by an interaction involving three single BHs (a "three-body binary" formation, Binney & Tremaine 2011). This result is surprising, given that three-body binary formation is expected to be the dominant mechanism for creating new

BBHs in the cores of GCs (Morscher et al. 2015). However, these three-body binaries are not necessarily the same binaries that will become future gravitational-wave sources. In order to be ejected from the cluster, this first generation of binaries must undergo several scattering encounters to pump up their gravitational binding energies–encounters that offer many opportunities to form new binaries by exchanging components. These gravitational encounters erase the original state of the first generation of BBHs, and become the primary mechanism for producing BBH mergers from GCs.
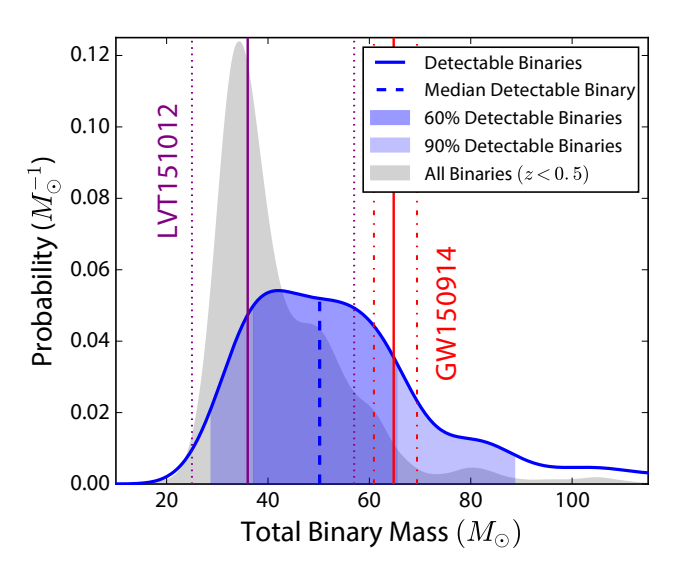

Figure 2. The distribution of BBH total masses from GCs. In gray, we show the distribution of all mergers that occur at $z < 0.5$ (for GCs that form at $z \simeq 3.5$), while in blue we show the distribution of sources detectable with Advanced LIGO during its first observing run. The median and 90% credible regions for the total mass of GW150914 are shown in red (The LIGO Scientific Collaboration & The Virgo Collaboration 2016b). We also show the gravitational-wave trigger, LVT151012, in purple (where we have computed the median and credible regions by adding the component mass median and 90% credible interval boundaries from The LIGO Scientific Collaboration & The Virgo Collaboration 2016a). Note that, while LVT151012 is below the threshold to be considered a detection, there exists a $\gtrsim 84\%$ chance that the signal was of astrophysical origin (Abbott et al. 2016c).

In addition to their formation, all 14 GW150914 progenitors were ejected from their host clusters after a strong interaction. This is consistent with Rodriguez et al. (2016), which found that 81% of BBHs ejected from a GC are ejected following a binary-single encounter, and 13% following a binary-binary encounter. We find that 9 of the 14 binaries were ejected from the cluster following an exchange encounter, in which pre-existing binary exchanged components and was ejected from the cluster before it could interact with other BHs (although the binary that was exchanged into may have

---

[1] Note that the proportionality constant in 1 can vary from ~ 10 to ~ 100 (in solar units) within a fixed cluster. See Rodriguez et al. (2016), Figure 2 and Equations 6-10.

Mergers	Pessimistic	Realistic	Optimistic
O1 (Detections / 16 Days)	0.05	0.2	0.7
O1 (Detections / 50 Days)	0.2	0.5	2
O2 (Detections / Year)	4	15	60
Design Sensitivity (Detections / Year)	30	100	400
Merger Rate at $z \sim 0.1$ (Mergers / Gpc^3 / Year)	2	5	20
Merger Rate at $z \sim 1$ (Mergers / Gpc^3 / Year)	4	10	40

Table 1. The expected merger rate for all BBHs from GCs. We show the theoretical detection rate for the first observing run of Advanced LIGO (O1) over a 16 day period (consistent with the GW150914 detection) and over a ∼50 day period (the length of O1, assuming a ∼ 4 month duration (Abbott et al. 2016b) with a double-coincident runtime fraction of 16/39 (Abbott et al. 2016c)). We also show the detection rate given the projected sensitivity for Advanced LIGO's second observing run (O2, with a proposed length of 6 months (Abbott et al. 2016b), for which we use the mid-sensitivity curve from Barsotti & Fritschel (2012)), and the final design sensitivity from Shoemaker (2009). Both projected rates assume a year of double-coincident data from both LIGO detectors. For reference, we show the total merger rate density from Rodriguez et al. (2016) at $z \sim 0.1$ (the observed redshift of GW150914) and at $z \sim 1$. The optimistic and pessimistic rates are computed assuming the $\pm 1\sigma$ uncertainties on the spatial density of GCs in the universe from Rodriguez et al. (2015), and considering all GCs to have initial virial radii of 1 pc or 2 pc, respectively. The realistic rate assumes the mean spatial density of GCs, and an even mix of 1 pc and 2 pc clusters.

undergone many encounters before ejection). The remaining 5 binaries were retained in the cluster after formation, and continued to interact with other BHs in the core until one such encounter ejected the BBH from the cluster. We show two examples of GW150914 formation histories in Figure 1, one in which the binary is ejected following an exchange encounter, and one in which the binary is formed and ejected after repeated scattering encounters.

Binaries that are ejected following an exchange interaction tend to be ejected from the cluster early, when there are still many $\sim 30 M_\odot$ BHs in the cluster. Conversely, systems that are ejected by repeated scatterings interactions tend to be ejected several Gyr later, when there are fewer BHs of comparable mass to produce an energetic exchange interaction. The distribution of inspiral times from both processes is nearly identical. But since we are only interested in GW150914-like binaries that merge in the local universe, we find that binaries ejected following an exchange are ejected early with longer inspiral times, while binaries ejected following several scattering interactions are ejected later with shorter inspiral times.

As Figure 1 makes clear, the dynamical history of any particular system is quite complex. But the interactions ensure that the orbital properties of dynamically-formed BBHs are a function only of well-understood gravitational processes, completely free of any dependence on the initial conditions of the BBH population. This eliminates many of the uncertainties associated with the modeling of isolated binary stellar evolution in galactic fields. The dynamical formation channel is largely independent of the many unconstrained parameters of binary evolution (e.g. the outcome of common envelope evolution) that can cause estimates of the BBH merger rate from the field to vary by several orders of magnitude

(Rodriguez et al. 2016).

4. DETECTION RATE

With this understanding of the dynamical formation scenario, it is only natural to ask: what masses of dynamically-formed BBHs are most likely to be detected by Advanced LIGO? The answer depends on two factors: the underlying distribution of BBH mergers in mass and redshift, and the sensitivity of the LIGO detector to BBH mergers with specific masses at a given redshift. In Figure 2, we show the distribution of BBH mergers from all our models, with the BBHs drawn randomly from specific GC models proportionally to the observed mass distribution of GCs (with clusters closer to the peak of the GC mass function contributing more BBH mergers to our effective sample, see Harris et al. 2014; Rodriguez et al. 2016, and Appendix B). Although there exist many mergers in the local universe ($z < 0.5$) with total masses from $20 M_\odot$ to $120_\odot$, the majority of mergers occuring in the present day lie in the peak between $30 M_\odot$ and $40 M_\odot$. This is consistent with Morscher et al. (2015); Rodriguez et al. (2016), which found that GCs process through their most massive BHs early, leaving behind the less-massive systems to form binaries and merge in the local universe. The peak at $\sim 35 M_\odot$ is primarily dominated by contributions from the $Z = 0.25 Z_\odot$ models, while the tail extending to high masses is primarily from low-metallicity ($Z = 0.05 Z_\odot$, $0.01 Z_\odot$) clusters. As with GW150914, our models show that mergers more massive that $40 M_\odot$ at low redshifts are most likely to have been formed in massive, low-metallicity clusters.

To translate this into a distribution and rate of detectable sources, we combine the total distribution of BBH mergers with the publicly-available Advanced LIGO sensitivity spectrum representative for the GW150914 observation (Kissel 2015) and a and com-

pute the distribution of detectable BBHs from GCs. We find that the median total mass of a BBH detectable during the 16 days of Advanced LIGO's first observing run (O1) is $50M_\odot$, with 60% of sources having total masses from $37M_\odot$ to $66M_\odot$ (enclosing the $65M_\odot$ total mass of GW150914), and 90% of sources having masses from $29M_\odot$ to $89M_\odot$. In Table 1, we integrate the mass distribution over all redshifts, and list the detection rate of BBH mergers from GCs for different current and planned observing runs of Advanced LIGO. We find that, during the first 16 days of O1, Advanced LIGO could have detected anywhere from 0.05 to 0.7 BBH mergers from GCs. Based on these results, we conclude that GW150914 is consistent with dynamical formation in a GC.

With only a single detection, and significant uncertainties on the BBH merger rate from isolated binary stellar evolution, it cannot be definitively said which of the many proposed formation channels produced GW150914. However, both GW150914 and the results presented here indicate that Advanced LIGO may detect many more BBH mergers in the near future (Abbott et al. 2016c). Once Advanced LIGO has produced a catalog of BBH merger candidates with different masses and spins at different redshifts, we will begin to constrain many of the existing BBH population models, yielding tremendous information about BH formation and dynamics across cosmic time.

REFERENCES

Abbott, B. P., Abbott, R., Abbott, T. D., et al. 2016, ApJL, 818, L22

Abbott, B. P., Abbott, R., Abbott, T. D., et al. 2016a, PhRvL, 116, 061102

—. 2016b, LRR, 19, 1

—. 2016c, astro-ph, arXiv:1602.03842

Ade, P. A. R., Aghanim, N., Arnaud, M., et al. 2015, astro-ph, arXiv:1502.01589

Antonini, F., Chatterjee, S., Rodriguez, C. L., et al. 2016, ApJ, 816, 65

Antonini, F., Murray, N., & Mikkola, S. 2014, ApJ, 781, 45

Barsotti, L., & Fritschel, P. 2012, Early aLIGO Configurations: example scenarios toward design sensitivity, Tech. Rep. LIGO-T1200307

Belczynski, K., Bulik, T., Fryer, C. L., et al. 2010, ApJ, 714, 1217

Belczynski, K., Bulik, T., Mandel, I., et al. 2013, ApJ, 764, 96

Belczynski, K., Buonanno, A., Cantiello, M., et al. 2014, ApJ, 789, 120

Bell, E. F., McIntosh, D. H., Katz, N., & Weinberg, M. D. 2003, ApJS, 149, 289

Binney, J., & Tremaine, S. 2011, Galactic Dynamics (Second Edition) (Princeton University Press), 920

Chatterjee, S., Rodriguez, C. L., & Rasio, F. A. 2016, astro-ph, arXiv:1603.00884

Dominik, M., Belczynski, K., Fryer, C., et al. 2013, ApJ, 779, 72

Finn, L. S. 1996, PhRvD, 53, 2878

Fregeau, J. M., Cheung, P., Portegies Zwart, S. F., & Rasio, F. A. 2004, MNRAS, 352, 1

Harris, W. E., Harris, G. L. H., & Alessi, M. 2013, ApJ, 772, 82

Harris, W. E., Morningstar, W., Gnedin, O. Y., et al. 2014, ApJ, 797, 128

Heggie, D. C. 1975, MNRAS, 173, 729

Hénon, M. 1971, Ap&SS, 14, 151

—. 1975, Dynamics of the Solar Systems, doi:1975IAUS...69..133H

Hurley, J. R., Pols, O. R., & Tout, C. A. 2000, MNRAS, 315, 543

Hurley, J. R., Tout, C. A., & Pols, O. R. 2002, MNRAS, 329, 897

Husa, S., Khan, S., Hannam, M., et al. 2016, PhRvD, D93, 44006

Kelvin, L. S., Driver, S. P., Robotham, A. S. G., et al. 2014, MNRAS, 439, 1245

Khan, S., Husa, S., Hannam, M., et al. 2016, PhRvD, D93, 44007

Kissel, J. 2015, H1 Calibrated Sensitivity Spectra Oct 1 2015 (Representative for Start of O1), Tech. Rep. LIGO-G1501223

MacLeod, M., Trenti, M., & Ramirez-Ruiz, E. 2016, ApJ, 819, 70

Mapelli, M., Zampieri, L., Ripamonti, E., & Bressan, A. 2013, MNRAS, 429, 2298

Moody, K., & Sigurdsson, S. 2009, ApJ, 690, 1370

Morscher, M., Pattabiraman, B., Rodriguez, C., Rasio, F. A., & Umbreit, S. 2015, ApJ, 800, 9

Morscher, M., Umbreit, S., Farr, W. M., & Rasio, F. A. 2013, ApJL, 763, L15

Portegies Zwart, S. F., & McMillan, S. L. W. 2000, ApJL, 528, L17

Rodriguez, C. L., Chatterjee, S., & Rasio, F. A. 2016, PhRvD, 93, 084029

Rodriguez, C. L., Morscher, M., Pattabiraman, B., et al. 2015, PhRvL, 115, 051101

Rodriguez, C. L., Morscher, M., Wang, L., et al. 2016, astro-ph, arXiv:1601.04227

Samsing, J., MacLeod, M., & Ramirez-Ruiz, E. 2014, ApJ, 784, 71

Scheepmaker, R. A., Haas, M. R., Gieles, M., et al. 2007, A&A, 469, 925

Shoemaker, D. 2009, Advanced LIGO anticipated sensitivity curves, Tech. Rep. LIGO-T0900288-v3

Spera, M., Mapelli, M., & Bressan, A. 2015, MNRAS, 451, 4086

The LIGO Scientific Collaboration, & The Virgo Collaboration. 2016a, astro-ph, arXiv:1602.03839

—. 2016b, astro-ph, arXiv:1602.03840

Vink, J. S. 2011, Ap&SS, 336, 163

APPENDIX

A. MONTE CARLO SIMULATIONS OF GLOBULAR CLUSTERS

Throughout this study, we use a series of 48 GC models, first created in Rodriguez et al. (2016), to explore the dynamical formation pathways of GW150914. These models were created with our Cluster Monte Carlo (CMC) code, a Hénon-style Monte Carlo approach to stellar dynamics (Hénon 1971, 1975). By assuming spherical symmetry, a large number of particles, and dynamics primarily driven by two-body relaxation, CMC can model GCs with significantly more single and binary objects than a direct N-body integration. Recent work (Rodriguez et al. 2016) has shown that CMC can model GCs with $N \sim 10^6$ particles with similar accuracy to state-of-the-art direct integrators, reproducing both the global cluster parameters and the BBH properties in a fraction of the time, allowing us to fully explore the parameter space of dense star clusters.
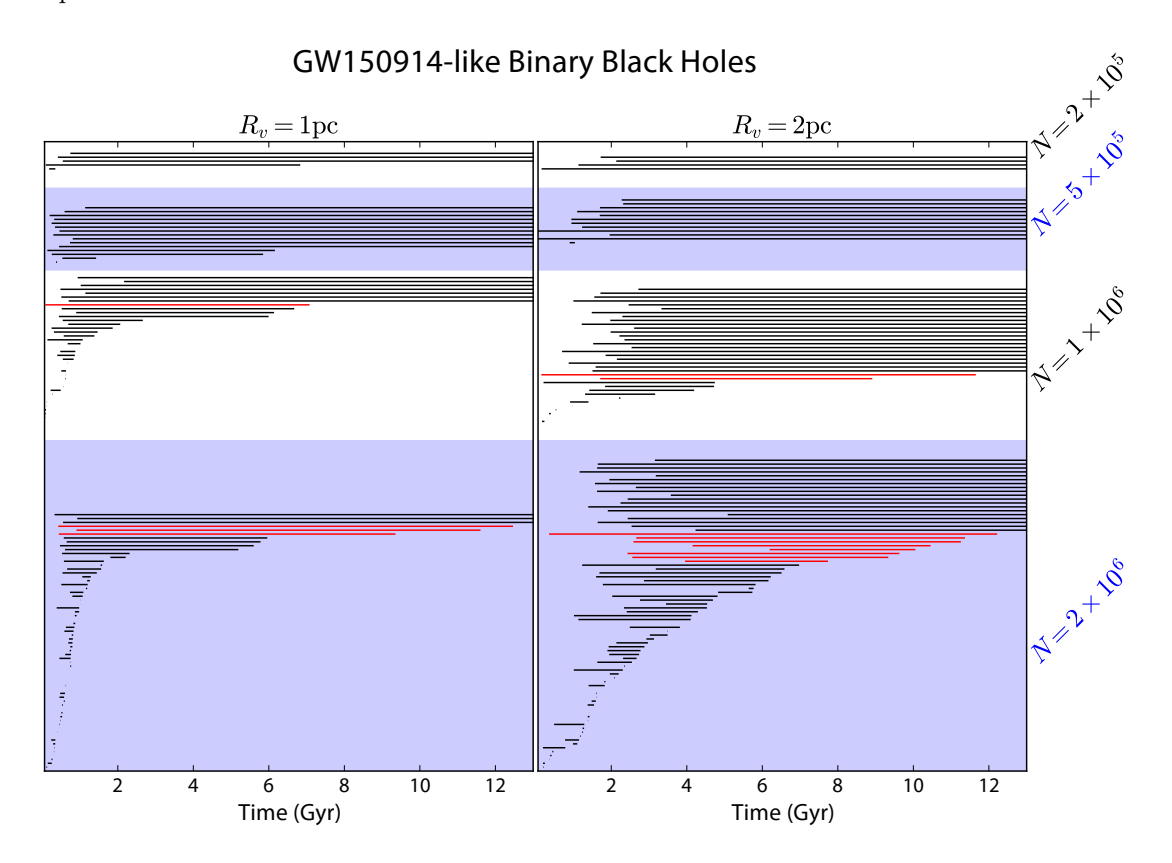

Figure A1. Graphical representation of all 262 BBHs with masses similar to GW150914 from the 48 GC models, sorted in order of increasing merger times. We separate the models according to their initial N and virial radii, such that each rectangle represents the BBHs from 6 models. The left end of each line indicates when each binary was ejected from the cluster and the right end indicates the merger time. Those binaries that merge in the local universe ($z < 0.5$, which we consider GW150914 progenitors) are indicated in red. As we consider more massive and more compact clusters, a larger number of BBHs will merge within a Hubble time, consistent with previous results (Rodriguez et al. 2016, Figure 1).

In addition to two-body relaxation, various improvements to CMC have incorporated much of the necessary physics to correctly treat the BBH dynamical formation problem. In particular, we consider:

- **three-body binary formation**, using a probabilistic prescription for three BHs that pass within a certain radius (Morscher et al. 2013),

- **strong three-body and four-body gravitational scattering encounters**, computed by direct summation of Newtonian gravity with the `Fewbody` integrator (Fregeau et al. 2004), and

- **single and binary stellar evolution**, using the BSE package for rapid stellar evolution (Hurley et al. 2000, 2002).

#	m_1 ($M_\odot$)	m_2 ($M_\odot$)	a (AU)	e	P_{orb} (days)	T_{ejec} (Gyr)	T_{insp} (Gyr)	Redshift (z)
1	38.5	26.4	0.30	0.53	7.45	0.42	12.04	–
2	37.6	25.4	0.25	0.44	5.75	0.44	8.92	0.21
3	32.0	31.6	0.25	0.37	5.72	0.91	10.70	0.03
4	35.3	30.5	0.40	0.74	11.39	0.08	7.00	0.46
5	35.5	25.8	0.21	0.13	4.49	0.15	11.51	0.02
6	37.6	30.1	0.77	0.89	29.99	1.70	7.20	0.26
7	36.3	28.2	0.57	0.82	19.57	0.35	11.87	–
8	32.9	32.3	0.40	0.75	11.44	2.56	6.78	0.21
9	32.6	32.1	0.30	0.58	7.46	2.59	8.67	0.05
10	32.7	28.6	0.37	0.78	10.50	6.20	3.86	0.15
11	35.1	32.5	0.22	0.13	4.58	2.66	8.71	0.05
12	33.4	27.5	1.32	0.96	70.97	3.95	3.79	0.38
13	32.2	28.2	0.38	0.76	11.01	4.15	6.30	0.12
14	32.9	31.3	0.25	0.50	5.70	2.43	7.20	0.19

Table A1. The 14 GW150914 progenitors identified from 48 GC models. We list the masses, orbital properties, and inspiral times for each binary at the moment it is ejected from the cluster. We also show the redshift of each merger, assuming all GCs to be exactly 12 Gyr old.

We have enhanced our stellar evolution prescriptions with new physics describing the distribution of remnant masses for BHs formed from core-collapsed massive stars, metallicity and temperature-dependent stellar winds, and the natal kicks of BHs. See Rodriguez et al. (2016) for details. These prescriptions are identical to those employed in the most recent estimates of BBH merger rates from galactic fields (Dominik et al. 2013), allowing us to directly compare our dynamical results to other channels for BBH formation. Note that we do not consider relativistic effects, such as post-Newtonian corrections to close dynamical encounters (Samsing et al. 2014) or long-term secular effects, such as Lidov-Kozai and gravitational wave emission in BH triple systems (Antonini et al. 2014; Antonini et al. 2016). Although these only contribute at the $\sim 1\%$, they should still be considered for any dynamically-complete treatment. We also assume that GCs do not contain intermediate-mass BHs which can influence the BBH formation and merger rate (e.g., MacLeod et al. 2016).

Our 48 cluster models are generated with a different number of initial particles, virial radii, and metallicities, in order to explore the full range of massive GCs observed in the Milky Way and other galaxies. We consider a grid with three different stellar metallicities ($Z = 0.25Z_\odot, 0.05Z_\odot$, and $0.01Z_\odot$), two different initial virial radii ($R_v = 1, 2$ pc) and four different initial particle numbers ($N = 2 \times 10^5, 5 \times 10^5, 1 \times 10^6, 2 \times 10^6$). Each set of initials conditions was run twice, with a different initial state of particle positions and velocities, for a total of 48 models. The details of these models can be found in Rodriguez et al. (2016).

Finally, we list the properties of the 14 GW150914 progenitors we consider in this study. In Table 2, we list the masses and orbital properties for each of the binaries, while in Table 3, we list the initial conditions of the clusters that created each BBH, and information about the dynamics of the binary inside the cluster. In Figure A1, we show all 262 BBHs from our models with masses similar to GW150914, highlighting in red those 14 BBHs that merge in the local universe.

B. GRAVITATIONAL WAVE DETECTABILITY

Computing the detectability of sources requires an understanding of both the sensitivity of the gravitational-wave detector and the underlying mass distribution of BBHs. Following Belczynski et al. (2014); Rodriguez et al. (2015), we write the detection rate per unit chirp mass as

$$\mathcal{R}(\mathcal{M}_c) = \int_0^\infty \mathcal{R}(\mathcal{M}_c, z) f_d(\mathcal{M}_c, z) \left(\frac{dV_c}{dz}\right) \left(\frac{dt_s}{dt_o}\right) dz \tag{B1}$$

where

- $\mathcal{R}(\mathcal{M}_c, z)$ is the rate of binary mergers at redshift z and chirp mass $\mathcal{M}_c$ from GCs in units of Mpc^{-3} $M_\odot^{-1}$ yr^{-1},

- $f_d(\mathcal{M}_c, z)$ is the fraction of detectable sources at a given chirp mass and redshift,

#	Metallicity ($Z_\odot$)	Particle Number	R_v (pc)	$N_{\text{part}}^{\text{prev}}$	N_{BS}	N_{BB}	Ejected By
1	0.05	2×10^6	1	0,5	1	0	BS (Exchange)
2	0.05	2×10^6	1	2, 0	1	0	BS (Exchange)
3	0.05	2×10^6	1	6, 1	12	3	BS
4	0.25	1×10^6	1	4, 1	1	0	BS (Exchange)
5	0.05	1×10^6	2	0, 1	1	0	BS (Exchange)
6	0.01	1×10^6	2	1, 11	0	1	BB (Exchange)
7	0.01	2×10^6	2	1, 0	1	0	BS (Exchange)
8	0.01	2×10^6	2	6, 1	3	1	BS
9	0.01	2×10^6	2	2, 5	0	1	BB (Exchange)
10	0.01	2×10^6	2	14, 1	1	2	BB
11	0.01	2×10^6	2	8, 4	1	0	BS (Exchange)
12	0.01	2×10^6	2	0, 12	3	0	BS
13	0.01	2×10^6	2	2, 0	8	0	BS
14	0.05	2×10^6	2	11, 5	1	0	BS (Exchange)

Table A2. The properties of the clusters that formed each GW150914 progenitor, and the dynamical interactions that formed each binary. For each, we show the number of previous binary partners each component had before finding its eventual GW150914 companion. We also show the number of binary-single and binary-binary encounters each binary underwent (including the interaction that created the binary). Finally, we list the type of encounter that ejected the binary from the cluster, and whether or not that encounter involved an exchange.

- $\left(\frac{dV_c}{dz}\right)$ is the comoving volume at a given redshift, assuming a flat ΛCDM cosmology with $\Omega_M = 0.306$ and $H_0 = 67.9\,\text{km}\,\text{s}^{-1}\,\text{Mpc}^{-1}$ (Ade et al. 2015), and

- $\left(\frac{dt_s}{dt_o}\right) \equiv \frac{1}{1+z}$ is the time dilation between a clock measuring the merger rate at the source and a clock on Earth.

To compute the merger rate, $\mathcal{R}(\mathcal{M}_c, z)$, we follow a similar procedure to Rodriguez et al. (2015); Rodriguez et al. (2016). We first assume that all GCs are exactly 12 Gyr old. The rate is then broken apart into three components:

$$\mathcal{R}(\mathcal{M}_c, z) \equiv \rho_{GC}\,\langle N_{\text{insp}}\rangle\,P(\mathcal{M}_c, z) \tag{B2}$$

where ρ_{GC} is the spatial density of GCs in the universe, which we assume to be $0.77\,\text{Mpc}^{-3}$, with an optimistic value of $2.31\,\text{Mpc}^{-3}$ and a pessimistic value of $0.32\,\text{Mpc}^{-3}$ based on recent measurements of galaxy luminosity functions (Kelvin et al. 2014) and the correlation between galaxy luminosity and GC number (Harris et al. 2013). See Rodriguez et al. (2015), supplemental materials, for details of the computation. We assume $0.77\,\text{Mpc}^{-3}$ to be the standard value, but consider the optimistic and pessimistic values better constrain the uncertainty of our estimate.

$\langle N_{\text{insp}}\rangle$ is the mean number of BBH mergers produced by a GC over 12 Gyr. This is found by creating a functional fit of the number of BBH mergers a cluster with a given present-day mass produces over its 12 Gyr lifetime. In Rodriguez et al. (2016), we found a relationship of the form $N_{\text{insp}}(M_{GC}) = N_{\text{BBH}}(M_{GC}) \times f_{\text{insp}}(M_{GC})$ to be satisfactory, where $N_{\text{BBH}}(M_{GC})$ is the linear relationship between the cluster mass and the total number of BBHs it produces and $f_{\text{insp}}(M_{GC})$ is the fraction of BBHs that will merge within 12 Gyr (which we fit to an error function[2]). We then determine $\langle N_{\text{insp}}\rangle$ by integrating the functional form of $N_{\text{insp}}(M_{GC})$ over the GC mass function, which we take to be a log-normal distribution with mean $\log_{10}(M_0) = 5.54$ and width $\sigma_M = 0.52$, based on recently-observed GC luminosity functions in brightest-cluster galaxies (Harris et al. 2014) and assuming a mass-to-light ratio of 2 for old stellar systems with minimal dark matter (Bell et al. 2003). As in Rodriguez et al. (2016), we compute three different values of $\langle N_{\text{insp}}\rangle$: the standard value (260 inspirals per 12 Gyr) determined by fitting $N_{\text{insp}}(M_{GC})$ to all 48 GC models, an optimistic value (347 inspirals per 12 Gyr), found when fitting only to clusters with $R_v = 1$ pc, and a pessimistic value (192 inspirals per 12 Gyr), found when considering only clusters with $R_v = 2$ pc. As with the values of ρ_{GC}, these estimates will be used to understand the uncertainties associated with our model assumptions.

---

[2] Chosen as a simple example of a cumulative distribution function, since the fraction of binaries that will merge within 12 Gyr goes from 0 to 1 as one considers clusters with larger masses. See Rodriguez et al. (2016), and Figure A1

We determine $P(\mathcal{M}_c, z)$, the probability distribution of mergers in chirp mass and redshift, by computing a 2D kernel density estimate (KDE) in $\mathcal{M}_c$ and binary merger time. The KDE was generated from our 48 GC models by sampling binaries at random from each model, appropriately reweighted to reproduce the mass distribution of GCs observed in the local universe. This is accomplished by selecting more binaries from models with larger weights, where the cluster weights are determined by evenly binning the log-normal GC mass function so that the average mass of models with the same initial particle number lies in the midpoint of each bin, then assigning to each model the integral of the GC mass function over that bin (normalized to the largest weight). We compute the weights separately for high- and low-metallicity clusters, as our high-metallicity models with $N = 2 \times 10^5$ disrupt before 12 Gyr and are excluded from the present analysis. In practice, this weighting scheme selects 100% of the binaries from our $N = 2 \times 10^6$ models, $\sim 55\%$ of the binaries from our $N = 5 \times 10^5, 1 \times 10^6$ models, and $\sim 35\%$ of the binaries from our $N = 2 \times 10^5$ low-metallicity models. Our parameter grid contains two low-metallicity clusters for every one high-metallicity cluster, so we further multiply the weights of the $Z = 0.05Z_\odot, 0.01Z_\odot$ models by 0.85 to ensure that we sample binaries from our models assuming that 56% of GCs are low-metallicity[3] (taken from the spatial densities of low- and high-metallicity clusters determined in Rodriguez et al. 2015, Supplemental Materials). Finally, we note that while the integral in equation B1 is performed in redshift, we compute the KDE with the merger times of the binaries. This is to ensure that $P(\mathcal{M}_c, z)$ is in units of $M_\odot^{-1}$ yr^{-1}. The distribution is then expressed in redshift by assuming $P(\mathcal{M}_c, z) = P_t\left(\mathcal{M}_c, t_{\mathrm{lookback}}(z)\right)$, using the stated cosmological parameters. Thus, $\mathcal{R}(\mathcal{M}_c, z)$ is in units of Mpc^{-3} M$_\odot^{-1}$ yr^{-1}.

To compute the detectability of sources, $f_d(\mathcal{M}_c, z)$, we assume a single Advanced LIGO detector and a minimum signal-to-noise ratio (SNR) of 8 for a detection (which is equivalent to a network SNR of 12, the current threshold for LIGO detections). The SNR for a face-on, directly over the detector, and optimally-oriented binary is defined as:

$$\mathrm{SNR} = \sqrt{4\Re \int_0^\infty \frac{|\tilde{\mathrm{h}}(\mathrm{f})|^2}{\mathrm{S_n(f)}} \mathrm{df}} \tag{B3}$$

where $\tilde{h}(f)$ is the gravitational wave in the frequency domain and $S_n(f)$ is the one-sided power spectral density of the detector noise. We compute $\tilde{h}(f)$ using the IMRPhenomD (Husa et al. 2016; Khan et al. 2016) gravitational waveform model[4] which covers the full BBH coalescence including the inspiral, merger, and ringdown phases. For our effective O1 observation, we use the publicly-available power spectral density released as part of the GW150914 observation (Kissel 2015), while our O2 and design sensitivity calculations used the noise curves cited in the main text. These optimal SNRs (which account for the dependence on redshift and chirp mass) are then multiplied by the antenna pattern function for a single detector, $\Theta(\alpha, \delta, \iota, \psi)/4$, which describes how the gravitational wave SNR decreases for different binary sky locations, inclinations, and polarizations (Finn 1996). The actual fraction of detectable sources, $f_d(\mathcal{M}_c, z)$, is determined by computing a Monte Carlo over the domain of Θ, and counting what fraction of sources at a given chirp mass and redshift have a detectable SNR > 8. See Belczynski et al. (2013, 2014) for a complete description.

What we show in Figure 2 is the normalized distribution from equation B1, where we convert from chirp mass to total mass by assuming all sources have equal-mass components. To compute the actual detection rate, we integrate equation B1 over all $\mathcal{M}_c$. Since each computation of $\mathcal{R}(\mathcal{M}_c, z)$ involves computing $P(\mathcal{M}_c, z)$, which is based on a random draw of inspirals from our models, we compute the integral of B1 with 100 independent sample of inspirals and report the mean of the results[5] For our optimistic and pessimistic assumptions, we use the $\pm 1\sigma$ values from the 100 independent draws, and employ the optimistic and pessimistic values of ρ_{GC} and $\langle N_{\mathrm{insp}} \rangle$ described above. Thus, the range of values reported do not represent a true statistical uncertainty on our models, but are intended to provide a reader with a better understanding of the astrophysical uncertainties associated with our assumptions. This procedure is similar to that developed in Rodriguez et al. (2015).

---

[3] Note that this is at odds with the observed distribution of GCs in the Milky Way, in which $\sim 75\%$ of GCs low-metallicity. However, we find that changing the metallicity fraction from 56% to 75% does not change the quantitative results for O1 quoted in the main text, and only changes the detection rates for design sensitivity LIGO at the $\sim 5\%$ level.

[4] This waveform model is available in the LALSimulation package of the LIGO Algorithm Library (LAL) software suite available

from https://wiki.ligo.org/DASWG/LALSuite.

[5] This is done mostly for completeness: our weighting scheme draws nearly all of the binaries from the most massive clusters (which produce the most binaries), so there is little variation between different independent samples. In practice, the uncertainty in our estimate is primarily dominated by the uncertainty in ρ_{GC}.